Biophysics, Vol. 47, No. 6, 2002, pp. 968–980. Translated from Biofizika, Vol. 47, No. 6, 2002, pp. 1044–1058.

CELL BIOPHYSICS

Kinetic Model of Primary Photosynthetic Processes in Chloroplasts. Description of the Fast Phase of Chlorophyll Fluorescence Induction under Different Light Intensities

G. V. Lebedeva[1], N. E. Belyaeva[1], O. V. Demin[2], G. Yu. Riznichenko[1], and A. B. Rubin[1]

[1]*Biological Faculty, Moscow State University, Moscow, 119899 Russia*
[2]*Belozersky Institute of Physico-Chemical Biology, Moscow State University, Moscow, 119899 Russia*

Received September 2, 2002

Abstract—A kinetic model was developed for generation and utilization of the transmembrane electrochemical proton gradient in primary photosynthetic processes in chloroplasts. The model gives a detailed description of the catalytic cycles in photosystems I and II, the cytochrome *b/f* complex, ATP synthesis, and passive leakage of H^+, K^+, and Cl^- through the thylakoid membrane. Account is taken of the dependence of the electron transport rate on the transmembrane potential. The model was tested for consistency with the experimental data on the fast phase of chlorophyll fluorescence induction under different light intensities (high to low). The composition of the fluorescence response was analyzed for each illumination level.

Key words: regulation, photosynthesis, mathematical model, fluorescence induction

INTRODUCTION

The information conveyed by chlorophyll fluorescence is commonly used to study the state of the plant photosynthetic apparatus [1–4]. In this regard, one of the most important effects is fluorescence induction, i.e., the change in the intensity of the fluorescence of a dark-adapted specimen developing upon exposure to constant illumination. This phenomenon was first reported in 1931 [5] and actively studied later [1–3, 6–8]. The induction curves thus registered reflect the process of plant adaptation to new illumination conditions, and are multiphasic (see inset in Fig. 1) because the photosynthetic system comprises processes with different characteristic times. At present, it is generally accepted to consider the following main phases and parameters of chlorophyll fluorescence induction: fast phase, whereby the fluorescence intensity rises from the initial level F_0 to the maximal F_P within a time on the order of seconds; and slow phase, whereby the fluorescence intensity relaxes to a certain steady state F_T within some tens of seconds. The pattern of the fast phase depends on the light intensity. Under low illumination there is usually one intermediate phase *I*, whereas under high illumination there are at least two, *J* and *I*.

In general, the fluorescence induction curve is an overall result of interaction of the processes of energy transduction and electron transfer along the photosynthetic chain. One can qualitatively collate separate components of the induction curve with particular processes that take place in the plant photosynthetic machinery (charge separation in the reaction center, generation of the transmembrane electrochemical proton potential, changes in the redox state of the plastoquinone pool, etc.). Indeed, all these processes are interconnected, and it is often hard to determine what contribution is made by each of them to the phasing of the induction curve. To interpret the experimental results, use is commonly made of the methods of mathematical modeling, permitting assessment of the photosynthetic processes that give rise to the induction effects [9–17]. The notions on the mechanisms of

Abbreviations: Chl, chlorophyll; Fd, ferredoxin; Pc, plastocyanin; Phe, pheophytin; PQ, plastoquinone; PQH_2 or QH_2, plastoquinol; PS, photosystem; WSC, water-splitting complex.

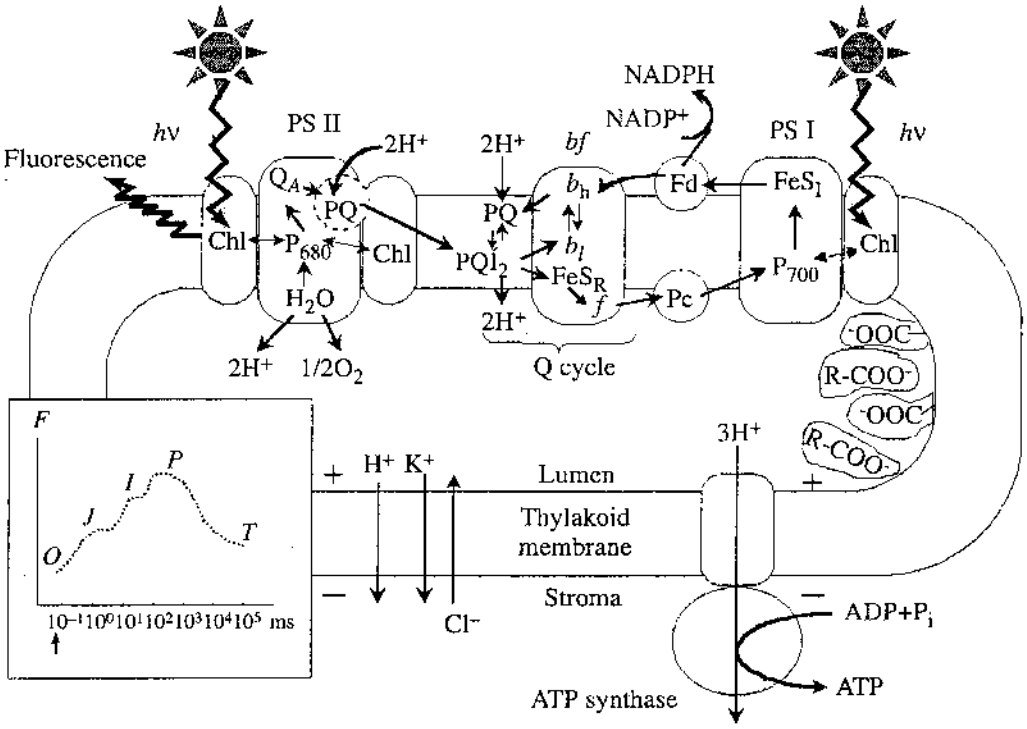

Fig. 1. Flowchart for the generalized model of primary photosynthetic processes. PS, photosystem; Chl, antenna chlorophyll; P680 and P700, pigments of the PS II and PS I reaction centers; FeS_I, acceptor complex of PS I; Fd, ferredoxin; Pc, plastocyanin; *bf*, cytochrome *b/f* complex; b_h and b_l, high- and low-potential hemes; FeS_R, Rieske iron–sulfur center; $R\text{-}COO^-$ designate buffer groups. Signs (+) and (–) on the membrane indicate that the thylakoid lumen is charged positively and the chloroplast stroma is charged negatively in the course of the photosynthetic processes. Solid zigzag arrows denote quanta of incident light and fluorescence/ Common arrows indicate the direction of electron transfer along the chain and the ion fluxes across the thylakoid membrane upon the onset of illumination. The inset schematically depicts the chlorophyll fluorescence induction curve with conventional phase designations; upward arrow at the abscissa axis marks light on.

photosynthetic processes laid into such models inevitably influence the interpretation of results obtained upon fitting the model parameters to the experimental data on chlorophyll fluorescence.

The simplifications introduced in most of the models describing the fast phase of the induction curve make them applicable only to certain 'particular cases' of experimental fluorescence curves. Thus chlorophyll fluorescence induction was assessed in the presence of an electron transfer inhibitor diuron, when the induction curve lacked intermediate phases. Some models [10–12] describe the fast phase under low illumination; other models [13, 19] were proposed for the same process under intense illumination.

Further, most of the models available are restricted to the processes in photosystem II, inasmuch as its chlorophyll makes the major contribution to the fluorescence under study. However, any such model thereby neglects other processes that can influence the parameters of primary photoreactions, in particular, generation of the transmembrane proton gradient $\Delta\mu_{H^+}$ with participation of the PS I complexes and cytochrome *b/f* complex, as well as processes dissipating $\Delta\mu_{H^+}$ such as ATP synthesis and passive leakage of H^+, K^+, and Cl^- ions.

We propose a generalized model of primary photosynthetic processes, integrating the main modern notions on the structure and function of the photosynthetic machinery of green plants. Separate aspects of the model have been discussed elsewhere [20–24]. In the framework of the model, we present a description of the fast phase of chlorophyll fluorescence induction as dependent on the kinetics of the main primary steps of photosynthesis in a broad range of illumination intensity.

DESCRIPTION OF THE MODEL

Our model of primary photosynthetic processes is compartmentalized, and describes the events taking place in the three main compartments of the

chloroplast: stroma, thylakoid membrane, and thylakoid lumen. The general scheme of the processes thus considered is given in Fig. 1.

Illumination initiates electron transfer along the electron transport chain with coupled transmembrane proton translocation from the chloroplast stroma into the thylakoid lumen, whereby an electrochemical proton gradient $\Delta\mu_{H^+}$ (with electric and concentration components $\Delta\psi$ and ΔpH) is created across the thylakoid membrane.

Generation of $\Delta\mu_{H^+}$ involves highly specialized pigment—protein complexes of photosystems I and II as well as the cytochrome *b/f* complex. The $\Delta\mu_{H^+}$ is utilized in ATP synthesis by ATP synthase, and is also spent in H^+, K^+, and Cl^- leakage through the energized thylakoid membrane and in drawing electrons off PS I through the ferredoxin:NADPH reductase reaction.

The model is kinetic, being a set of ordinary differential equations that for every moment of time determines the state of the system of chemical reactions under study, i.e., gives the concentrations of the metabolites of the aggregate of reactions as functions of time. These balance equations are written as

$$\frac{dX_i}{dt} = v_{prd}(X_i) - v_{cns}(X_i), \qquad (1)$$

where X_i is the concentration of the ith metabolite in mM, $v_{prd}(X_i)$ and $v_{cns}(X_i)$ are the overall rates of its production and consumption, mM/s.

The photosynthetic electron transport chain includes mobile carriers (plastoquinone PQ, plastocyanin Pc, ferredoxin Fd) as well as carriers grouped in pigment—protein complexes of PS I, II, and *b/f*. It is known that acting mass equations are inapplicable to describing electron transfer between carriers within an integral complex [25–27]. Therefore, to consider the processes within the PS I, II, and *b/f* complexes, we resorted to an approach based on detailed description of the catalytic cycles for each such complex. The latter was described as a set of possible states, the number of which is determined by the number of electron carriers entering into the composition of the complex and the number of possible redox states of each carrier (e.g., excited, oxidized, reduced). Type (1) equations were written down for every possible state of the complex, with the variables X_i meaning the probability of the ith state of complex multiplied by the overall concentration of the given complex in the system.

Electron transfer from a pigment—protein complex to a mobile carrier was described by acting mass equations with bimolecular rate constants, taking the complex concentration to be equal to the sum concentration of its states capable of participating in the given electron transfer step.

In our model, the reaction rates are functions of variables involved in the given step as well as functions of model parameters. Evaluating the parameters of each reaction, account was taken of the relation between the rate constant of the forward and reverse reactions through the equilibrium constant:

$$k_i = k_{-i} K_{eq}^i. \qquad (2)$$

The equilibrium constants of redox reactions were determined from the experimental data on midpoint redox potentials:

$$K_{eq} = \exp\left(\frac{\Delta E_m}{RT / nF}\right), \qquad (3)$$

where ΔE_m is the difference of midpoint redox potentials measured relative to a standard hydrogen electrode, and n is the number of electrons transferred in the course of the redox reaction. The ΔE_m values were taken from the literature [28–31]. The equilibrium constant values calculated with equation (3) were used only as preliminary estimates, because the ΔE_m for a redox pair is usually measured under special conditions far from those *in vivo*. Therefore, some K_{eq} had then to be changed to improve the fit between the calculated and experimental data on fluorescence induction.

Dependence of Reaction Rate on Transmembrane Electric Potential

Any reaction step involving electric charge transfer across a membrane produces a transmembrane electric potential $\Delta\psi$, which, in its turn, influences the rate of electron transfer along the electron carrier chain [32–34]. The model takes this into account as the corresponding dependences of equilibrium and rate constants on $\Delta\psi$ as follows:

$$K_{eq}(\Delta\Psi) = \exp(-\alpha\Delta\Psi / (RT / F))K_{eq},$$

$$k_-(\Delta\Psi) = \exp(-\delta\alpha\Delta\Psi / (RT / F))k_+,$$

$$k_-(\Delta\Psi) = \exp((1-\delta)\alpha\Delta\Psi / (RT / F))k_-.$$

Here α is the portion of $\Delta\psi$ that is generated at the particular step by charge transfer across the membrane; δ is the portion of the membrane potential $\alpha\Delta\psi$ that affects the rate of the direct reaction; K_{eq}, k_+, and k_- are the corresponding constants at $\Delta\psi = 0$.

The electric membrane potential $\Delta\psi$ is a model variable, its time dependence is described by a differential equation

$$\frac{c_m}{F}\frac{d(\Delta\Psi)}{dt} = v(q_{lumen}) - v(q_{stroma}),$$

where c_m is the specific capacitance of the thylakoid membrane, F is the Faraday constant, and $v(q)$ are the rates of charge bulk density production, measured in mM and dependent on H^+, K^+, and Cl^- concentrations in the respective compartments.

The concentration component (ΔpH) of the proton electrochemical potential is also a model variable, determined at every moment by the difference in proton concentrations in the stroma and in the lumen.

Buffer Properties of Lumen and Stroma

The chloroplast stroma and the thylakoid lumen are known to exhibit buffer properties owing to the presence of various proton-binding groups in their volume. In our model, we approximate the buffering in these compartments with three proton-binding groups (B_1, B_2, B_3), their pK for protons varying from 4 to 8. The dissociation constants and the concentrations of buffering groups were chosen so as to fit the experimental data on the buffer capacity of the thylakoid lumen [35].

Consumption of the Transmembrane Electrochemical Potential $\Delta\mu_{H^+}$

In our model, the $\Delta\mu_{H^+}$ is utilized in ATP synthesis by ATP synthase, and is also spent in passive leakage of H^+, K^+, and Cl^- through the thylakoid membrane. The rate equation for the ATP synthase reaction is based on the minimal kinetic scheme of ATP synthesis/hydrolysis [34, 36, 37]. The dependence of proton leakage on the potential has been obtained [36, 38—40] within the framework of Eyring's model of ion transport through a three-barrier channel. The same mechanism was used to describe the electrogenic transmembrane transport of Cl^- and K^+.

Photosystem II

In our model, PS II is regarded as a membrane enzyme that under the action of light catalyzes reduction of plastoquinone to plastoquinol and creates a transmembrane electrochemical proton potential $\Delta\mu_{H^+}$ (Fig. 2). A detailed description of the PS II model has been given elsewhere [23].

Every kinetic state of PS II is determined by the states of its four constituent electron carriers: chlorophyll P680, pheophytin Phe, primary one-electron covalently bound quinone acceptor Q_A, and binding site for the secondary quinone acceptor Q_B. It is assumed that the excitation energy initially localized on one of the antenna pigments is rapidly (within picoseconds) equilibrated over the entire pool of PS II antenna pigments including the P680 reaction center pigment [2, 3, 41]. Therefore, the designation Chl covers the whole complex of these pigments.

Kinetic states x_i, y_i, z_i, g_i ($i = 1, 2, \ldots 7$) differ in the state of the Q_B binding site: in g_i the site is vacant, in x_i the site contains nonreduced Q_B, in y_i and z_i the PQ in the site carries one (Q_B^-) and two electrons (Q_B^{2-}), respectively.

Without illumination (dark adaptation) the PS II complex acquires states x_1 and g_1, which come into equilibrium (step 34). When the light is switched on, P680 goes into excited state (steps 1 and 28), which may be accompanied by primary (steps 2 and 29) and secondary (steps 3 and 30) charge separation. The water-splitting complex reduces the oxidized reaction center pigment (steps 4 and 31). We did not consider the molecular mechanism of the WSC operation, but assumed that per every electron passed from WSC to oxidized P680 there is one proton released into the intrathylakoid space. Thus, the sequence of steps 1–4 or 28–31 results in formation of "closed" reaction centers with reduced Q_A (states x_5 and g_5).

Further illumination of closed RC may result in repeated excitation of the pigment (steps 5 and 32) and primary charge separation (steps 6 and 33). Thereby arise the PS II states with oxidized pigment and reduced Phe and Q_A (states x_7 and g_7).

In any state g_i ($i = 1, \ldots 7$), PQ can bind in the Q_B site (steps 34–40) to give the corresponding states x_i ($i = 1, \ldots 7$). The bound Q_B is a two-electron carrier and can consecutively accept two electrons from Q_A^-. Steps 7 and 14 describe the transfer of the first and the second electron to Q_B with formation of states y_1 and z_1. Under light, these states can undergo the sequence of conversion described for x_1 and g_1, including pigment excitation (steps 8 and 15), primary

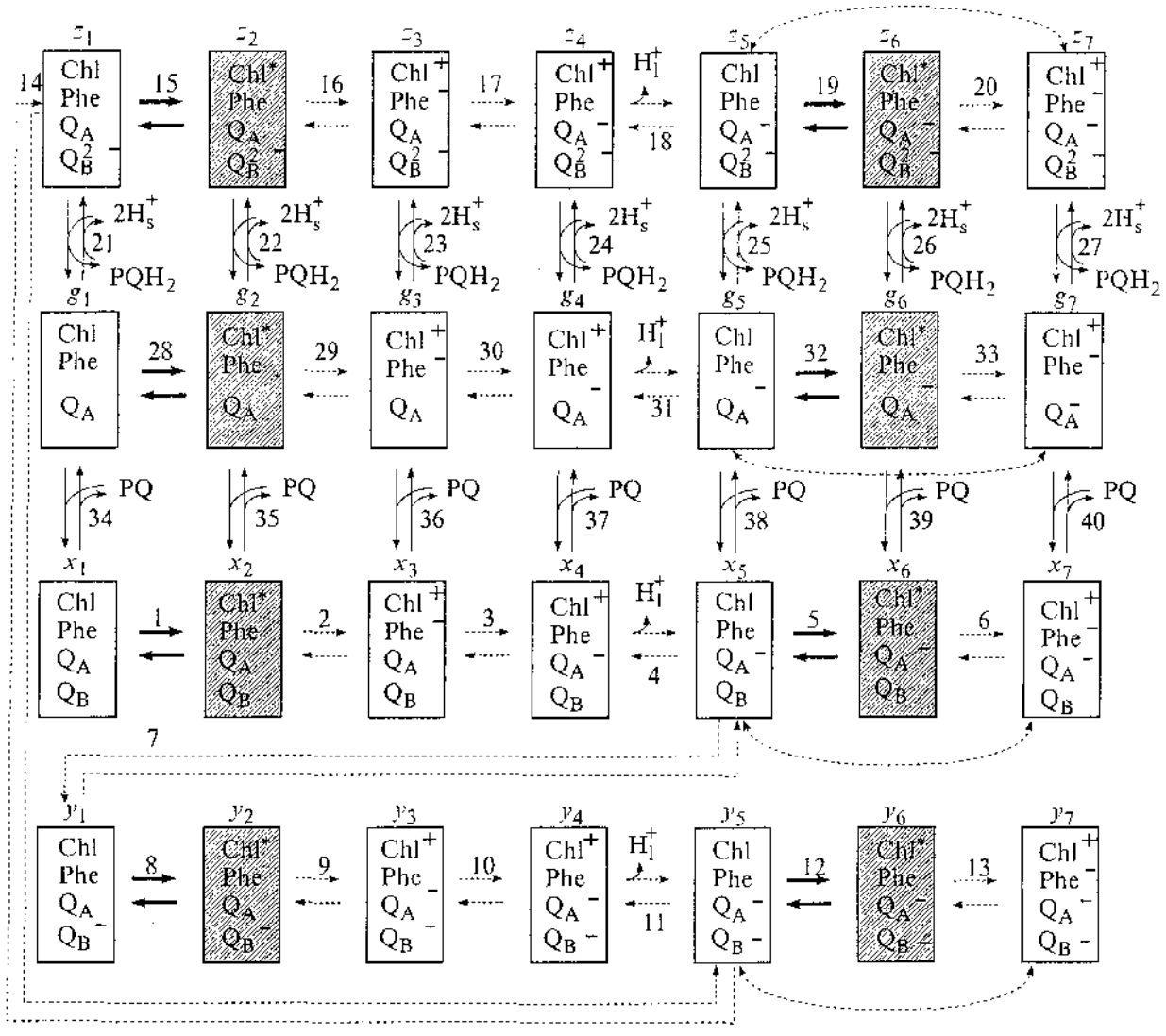

Fig. 2. The catalytic cycle of photosystem II. Each rectangle represents a particular kinetic state determined by the redox state of its constituent electron carriers. Shaded are the states capable of emitting fluorescence quanta. Chl, the total PS II chlorophyll including the antenna and the P680 pigments; Phe, pheophytin; Q_A and Q_B, primary and secondary quinone acceptors; PQ, plastoquinone; PQH_2, plastoquinol; H_l^+ and H_s^+ are protons released into the lumen and taken up from the stroma, respectively. Dotted arrows denote the fast steps (characteristic time less than 0.1 ms), continuous arrows denote the slow steps (characteristic time at least 1 ms), bold arrows mark the light steps. Numbers at the arrows and designations at the tops of the boxes correspond to the step numbers and model variables.

(steps 9 and 16) and secondary (steps 10 and 17) charge separation, reduction of oxidized P680 by WSC (steps 11 and 18), and excitation of closed RC (steps 12 and 19) attended by primary charge separation (steps 13 and 20).

In any state z_i (i = 1, ... 7), plastoquinol PQH_2 may be released (after uptake of two protons H_s^+) from the chloroplast stroma, giving states g_i (i = 1, ... 7) with vacant Q_B site (steps 21–27), and this closes the catalytic cycle of PS II.

Steps 1, 5, 8, 12, 15, 19, 28, and 32 marked with bold arrows in the scheme are the light steps, describing the transition of Chl into the excited state Chl* (light constant $k_L = k_i$ where i = 1, 5, 8, 12, 15, 19, 28, 32) and the reverse process of deactivation of the excited state with emission of fluorescence quanta (fluorescence constant $k_F = k_{-i}$ where i = 1, 5, 8, 12, 15, 19, 28, 32).

To calculate and compare the fluorescence yields under different light intensities, we used the function F presented as a sum concentration of PS II

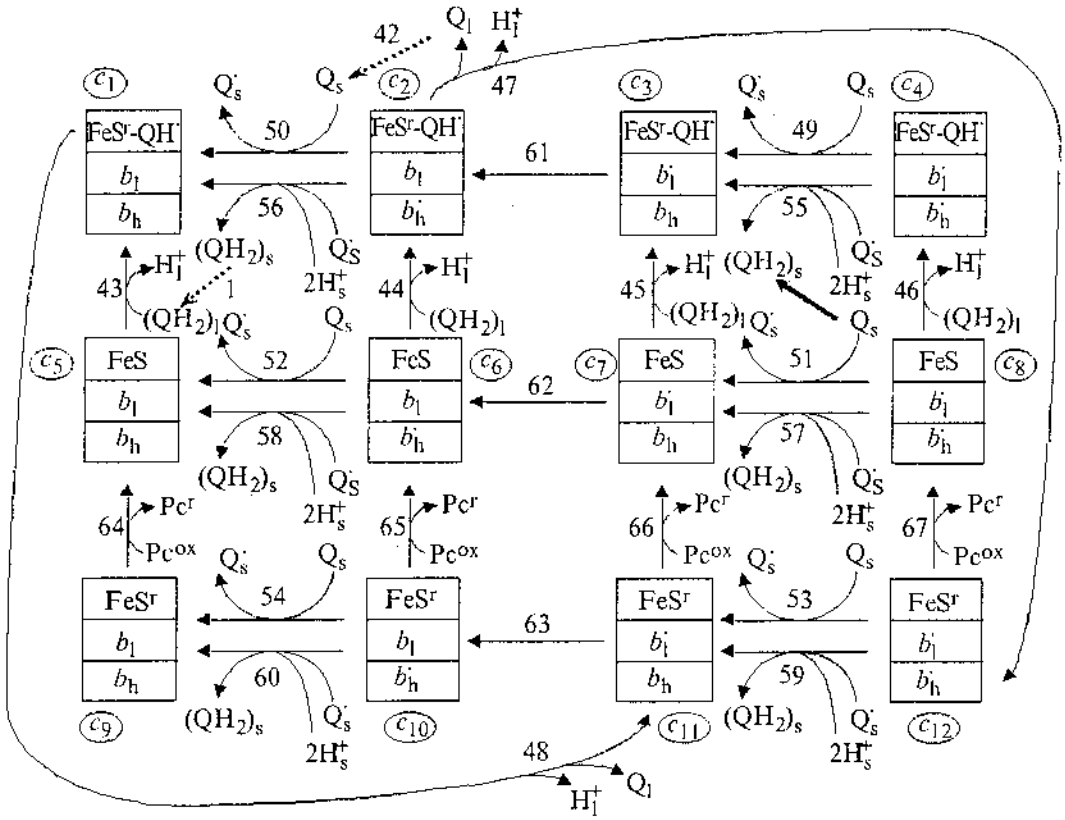

Fig. 3. The catalytic cycle of the cytochrome *b/f* complex. Each rectangle represents a particular kinetic state determined by the redox state of its constituent electron carriers. Superscripts mark the reduced (r) and oxidized (ox) states. Designations in ovals correspond to the model variables.

fluorescing states (i.e., states with excited Chl*) multiplied by the ratio of fluorescence and light constants:

$$F = \frac{k_F}{k_L}(x_2 + y_2 + z_2 + g_2 + x_6 + y_6 + z_6 + g_6). \quad (4)$$

Cytochrome *b/f* Complex

The cytochrome *b/f* complex was regarded as a membrane enzyme catalyzing electron transfer from plastoquinol to plastocyanin coupled with proton transport from the stroma into the thylakoid lumen. The corresponding aggregate of redox reactions is known as the Q cycle and is presented in Fig. 3.

The *b/f* complex has two catalytic centers—luminal (p) and stromal (n)—involved in the redox conversions of PQ [29]. In our model, the electrons are fed into the Q cycle (bold arrow without number in Fig. 3) via the reaction of Q reduction to QH_2 by PS LL (steps 21–27 in Fig. 2). This process takes place at the stromal (s) surface of the thylakoid membrane, after which plastoquinol diffuses to the luminal (l) side of the membrane (step 41, dotted arrow in the left-hand part of Fig. 3). Upon binding with the (p) center of the *b/f* complex, the plastoquinol passes one electron to the Rieske iron–sulfur center (FeS) and releases one proton into the thylakoid lumen; this makes a complex of protonated PQ with reduced FeS (steps 43, 44, 45, 46 depending on the redox states of FeS and the cyt *b* hemes). If the low-potential heme of cyt *b* is reduced, the semiquinone remains bound at the Rieske center until b_l is oxidized (in steps 49, 55, and 61). Then the second proton is released, and the semiquinone of the FeS^r-QH$^\cdot$ complex gives the electron to the b_l heme, thus converting into free PQ (steps 47 and 48), and diffuses back to the stromal side (step 42, dotted arrow in the upper part of the scheme). Further, the electron is transferred across the membrane from the low-potential to the high-potential heme (steps 61–63). Thereupon the reduced $b_h^\cdot$ heme reduces the PQ in the (n) center to produce semiquinone $Q_s^\cdot$ (steps 49–54). This semiquinone takes the second electron from b_h to become a plastoquinol through consuming two protons from the stroma (steps 55–60). Simultaneously, the electron accepted by the FeS center is transferred

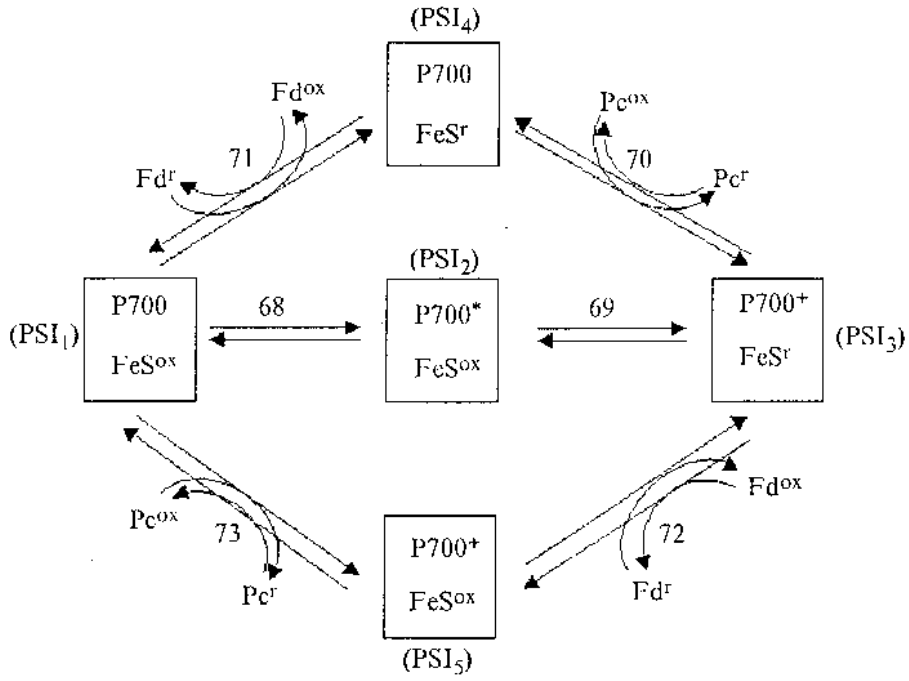

Fig. 4. Electron transfer in photosystem I. P700 is the reaction center chlorophyll, FeS here means the entire acceptor complex; Fd, ferredoxin; Pc, plastocyanin; superscripts mark the reduced (r) and oxidized (ox) states. (PSI_i) correspond to the model variables.

to cyt *f* and then to Pc (steps 64–67). The scheme does not show the step corresponding to electron transfer between Fe S and cyt *f*, because these carriers are in fast equilibrium (both rate constants $>10^5$ s^{-1}, equilibrium constant about 3 [29]).

We assumed that the Q cycle has four electrogenic steps: the first one corresponds to transmembrane electron transfer from b_l to b_h (61–63), and the other three correspond to proton transport in plastoquinone reduction (55–60) and plastoquinol oxidation (43–48). The interheme electron transfer was taken to be responsible for 80% of the overall electrogenesis, and the remaining 20% were shared equally between the proton-transport steps, which is in accord with the data [42, 43] obtained for the cytochrome bc_1 complex of purple bacteria.

Photosystem I

We regarded PS I as a membrane enzyme that under the action of light catalyzes oxidation of plastocyanin and reduction of ferredoxin. The scheme of the PS I catalytic cycle is given in Fig. 4. In our model we considered five possible kinetic states of PS I, which are determined by the state of the P700 reaction center pigment and the FeS acceptor complex. Note that FeS here designates the entire complex of acceptors: primary and secondary A_0 and A_1 as well as the iron–sulfur clusters F_x, F_A, and F_B. We did not go into details of electron transfer within the FeS complex, but assumed that the latter can be in two states, oxidized and reduced. This simplification appears expedient, because the electron transfer along the A_0–A_1–F_x chain is very rapid (10^{-12} to 10^{-9} s) [30]. Again, PS I comprises only one-electron carriers, which implies a simpler kinetic behavior of the system as compared with PS II.

Under light, the P700 passes into excited state P700* (step 68), with subsequent charge separation (step 69) and formation of state $P700^+FeS^r$. This state can further be 'utilized' in two ways. Oxidized $P700^+$ may first accept an electron from Pc (step 70), after which the acceptor complex will reduce Fd (step 71); or vice versa, first the reduced FeS complex may give its electron to Fd (step 72) and then Pc will reduce the oxidized P700 (step 73).

Table 1 lists the values for the model parameters. Estimation of the rate constants is a separate problem. Some values can be determined accurately enough (for instance, the rate constants for charge separation in PS II) owing to the vast experimental material accumulated. Other processes are less studied, and the literature data on their parameters are

Table 1. Model parameters*

Direct reaction rate constant (s^{-1})		Reverse reaction rate constant (k, s^{-1}) or equilibrium constant (K)	
$k_1 = k_5 = k_8 = k_{12} = k_{15} = k_{19} = k_{28} = k_{32}$	15; 150; 1500 depending on illumination	$k_{-1} = k_{-5} = k_{-8} = k_{-12} = k_{-15} = k_{-19} = k_{-28} = k_{-32}$	$3*10^8$
$k_2 = k_9 = k_{16} = k_{29}$	$3.3 \cdot 10^{11}$	$K_2 = K_9 = K_{16} = K_{29}$	2000
$k_3 = k_{10} = k_{17} = k_{30}$	$5 \cdot 10^9$	$K_3 = K_{10} = K_{17} = K_{30}$	10^6
$k_4 = k_{11} = k_{18} = k_{31}$	5000	$K_4 = K_{11} = K_{18} = K_{31}$	100
$k_6 = k_{13} = k_{20} = k_{33}$	$3.3 \cdot 10^{11}$	$K_6 = K_{33}$	200
k_7	2500/4348	K_7	20
k_{14}	2174	K_{14}	10
$k_{21} = k_{22} = k_{23} = k_{24} = k_{25} = k_{26} = k_{27}$	500	$K_{21} = K_{22} = K_{23} = K_{24} = K_{25} = K_{26} = K_{27}$	5
$k_{34} = k_{35} = k_{36} = k_{37} = k_{38} = k_{39} = k_{40}$	100	$K_{34} = K_{35} = K_{36} = K_{37} = K_{38} = K_{39} = K_{40}$	1
k_{41}	25		
k_{42}	25		
$k_{43} = k_{44} = k_{45} = k_{46}$	500	$K_{43} = K_{44} = K_{45} = K_{46}$	2.4
$k_{47} = k_{48}$	$2 \cdot 10^5$	$K_{47} = K_{48}$	10
$k_{49} = k_{51} = k_{53}$	200	$K_{49} = K_{51} = K_{53}$	2.5
$k_{50} = k_{52} = k_{54}$	100	$K_{50} = K_{52} = K_{54}$	2.5
$k_{55} = k_{56} = k_{57} = k_{58} = k_{59} = k_{60}$	25	$K_{55} = K_{56} = K_{57} = K_{58} = K_{59} = K_{60}$	400
$k_{61} = k_{62} = k_{63}$	10^3	$K_{61} = K_{62} = K_{63}$	100
$k_{64} = k_{65} = k_{66} = k_{67}$	2000	$K_{64} = K_{65} = K_{66} = K_{67}$	10
k_{68}	7.5; 75; 750 depending on illumination	k_{-68}	10^5
k_{69}	$2 \cdot 10^7$	K_{69}	10^4
$k_{70} = k_{73}$	10^3	$K_{70} = K_{73}$	100
$k_{71} = k_{72}$	10^6	$K_{71} = K_{72}$	1000

* Constants numbered as the reaction steps in Figs. 2–4.

contradictory. This particularly regards the slower processes such as PQ diffusion in the thylakoid membrane as well as transmembrane ion transport and the buffer properties of lumen and stroma. In this connection, most of the equilibrium and rate constants for the reactions considered in the model were averaged from the literature. At the same time, some parameters were optimized so as to attain a satisfactory fit to the experimental results.

RESULTS

The data below were obtained by solving numerically the set of model equations using the SCAMP package in a Pentium-II PC.

The model of primary photosynthetic processes in plant chloroplasts was used to calculate the theoretical curves of chlorophyll fluorescence induction at different light intensities. The latter were set with

Table 2. Stationary values of model variables for the dark-adapted object ($k_i = 0$, $i = 1, 5, 8, 12, 15, 19, 28, 32$)

x_1	1.34	Pc^{ox}	3.24
x_i, $i = 2, \ldots 8$	0.0	H_l^+	$10^{-3.6}$ (pH 6.6)
g_1	0.28	H_s^+	$10^{-4.1}$ (pH 7.1)
y_i, $i = 1, \ldots 8$	0.0	K_l^+	120
z_i, $i = 1, \ldots 8$	0.0	K_s^+	30
c_5	1.62	Cl_l^-	10
c_i, $i = 1, \ldots 12$; $i \neq 5$	0.0	Cl_s^-	30
PSI_1	1.62	Fd^r	0.0
PSI_i, $i = 2, \ldots 5$	0.0	Fd^{ox}	8.0
PQ_l	4.86	ATP	0.5
PQ_s	4.86	ADP	9.5
PQH_{2l}	0.0	P_i	40
PQH_{2s}	0.0	NADP	1.0
Pc^r	0.0	NADPH	0.0

appropriate values of light constants k_i ($i = 1, 5, 8, 12, 15, 19, 28, 32, 68$) and corresponded to 15, 150, or 1500 quanta per second per PS II reaction center. The relative fluorescence yield at every moment after the onset of illumination was calculated according to equation (4).

To model the changes in the state of the photosynthetic system after switching on the light, we had to choose the initial values of the variables that would correspond to the 'dark' state of the object. To this end, the stationary solution for the system was obtained in the case when all light constants were zero, and the resulting set of values was taken as the initial in all further calculations (Table 2). The data listed in Table 2 pertain to average chloroplast volume 40 μm^3; P700 content 2 mmol per 1 mol chlorophyll; and chloroplast stroma, thylakoid lumen, and thylakoid membrane volume ratio 10:1:1. The stoichiometry of PS II, *b/f*, PS I complexes, PQ, and Pc in the thylakoid membrane was taken to be 1:1:1:6:2.

As evident from Fig. 5, the model provides a good fit to the available experimental data on fluorescence induction under different illumination conditions. At small values of the light constants corresponding to low illumination (1%), fluorescence reaches its maximum in about 1–2 s, and the induction curve exhibits one intermediate phase (shoulder) at about 200 ms. A tenfold increase of the light constants, corresponding to medium illumination (10%), brings about a rise in the signal amplitude and shortens the time to the maximum (about 500 ms); the intermediate phase is less pronounced. At high light constants (intense illumination, 100%) fluorescence reaches its peak in 100–200 ms, with two intermediate phases (*J* about 2 ms and *I* about 20 ms).

To elucidate the nature of individual kinetic components of the initial part of the induction curve, we plotted the time dependences of the concentrations of PS II states capable of emitting fluorescence quanta (the 2nd and the 6th forms shaded in Fig. 2). Modeling revealed that at any light intensity the contribution of the states with oxidized Q_A (2nd forms) to the fluorescence is several orders of magnitude smaller than the contribution of the states with reduced Q_A (6th forms). This is in accord with the existing notion that overall fluorescence is proportional to the concentration of closed (i.e., Q_A^--containing) reaction centers of PS II [13]. For this reason, in further analysis of the fluorescence induction curves we can restrict ourselves to considering the kinetics of the PS II fluorescing states with reduced Q_A (x_6, g_6, y_6, z_6).

As demonstrated in Fig. 6b, the relative contribution of each fluorescing form depends on the light intensity. Thus under low illumination fluorescence is mostly emitted by states g_6 (the quinone acceptor with reduced Q_A and vacant Q_B) and z_6 ($Q_A^- Q_B^{2-}$). Indeed, these states are generated in the light from g_5 and z_5 which do not allow electron transfer from Q_A along

the chain (secondary acceptor either absent or fully reduced). As PQ attachment to the Q_B site and PQH_2 dissociation therefrom are relatively slow processes, states g_5 and z_5 (and hence g_6 and z_6) can accumulate to greater concentrations than the corresponding x and y, in which the secondary acceptor is not fully reduced and the Q_A^- electron can be transferred to Q_B to yield respectively y_1 and z_1. When the light is weak, this process prevails over formation of the excited states, so that fluorescing forms x_6 and y_6 are minor.

Under moderate illumination, the fluorescence of the system is also largely determined by the sum of g_6 and z_6, though the fraction of x_6 and y_6 increases somewhat.

Under intense illumination, the contribution of x_6 and y_6 to the fluorescence is comparable to that of g_6 and z_6, because the characteristic time of the formation of the excited states becomes close to the time of electron transfer from Q_A to Q_B. The fluorescence induction curve exhibits two distinct intermediate phases J and I; the former is provided by x_6 and y_6 and the latter is provided largely by z_6, while g_6 contributes to both.

The analysis of the kinetic components of the fluorescence induction curve allows some conclusions concerning the origin of its phases J, I, and P. The fluorescence peak P corresponds in time to attaining the maximal sum concentration of PS II fluorescing states with "fully closed' quinone acceptor complex (g_6 and z_6). Phase I is quite distinct at any illumination intensity, and the time to this phase shortens with increasing light intensity. As can be seen in Figs. 6a and 6b, the onset of this phase roughly corresponds to the appearance of an intermediate maximum on the curve for the z_6 content. Phase J is clearly discerned only under intense enough light, and is associated with accumulation of fluorescing states in which the acceptor is not fully reduced (not more than one electron on Q_B).

Collation of the modeling results for different light intensities leads to a conclusion that under all conditions the induction curve features all kinetic components, but they are pronounced to a varying extent and appear at varying times. Indeed, the overall fluorescence at every moment is determined by the sum of fluorescent signals emitted by different redox states of PS II (eight in our model), and all these states are present in the system under any illumination, but the fractions of each state and the time to

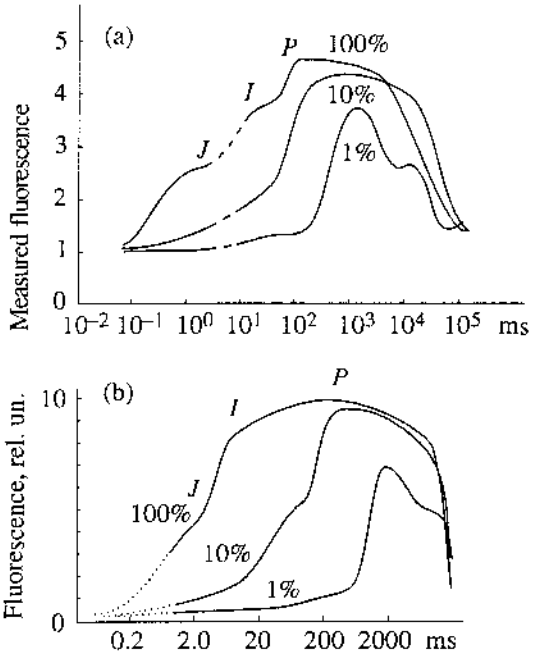

Fig. 5. Chlorophyll fluorescence induction curves at different light intensities. (a) Experimental data obtained upon illumination of dark-adapted pea leaves with red (650 nm) light at (100%) 600, (10%) 60, and (1%) 6 W/m^2; cited from [44]. (b) Calculations with the proposed model for illumination at (100%) 1000, (10%) 100, and (1%) 10 W/m^2, setting the PS II light constants to 1500, 150, and 15 s^{-1}.

peak concentration change with the frequency at which the light quanta get into the reaction center.

Of special interest are the causes of nonmonotone behavior of the z_6 content, which gives rise to the I phase on the induction curve.

Noteworthy is the correlation of the additional z_6 maximum with the 'second wave' of the transmembrane electric potential $\Delta\psi$; this is most clearly seen at low values of the light constants (Fig. 6a). The literature reports experiments on registering what is known as the "slow phase of electrochromic changes" in the absorption of light by carotenoids (whose spectrum is sensitive to electric field) upon illuminating the object with a train of flashes. The observed 'slow' (10–20 ms) changes in pigment absorption reflecting the $\Delta\psi$ shift are conventionally attributed to electrogenic electron transfer beyond the photochemical reaction centers of PS II. Thus considered were the roles of the *b/f* complex [29, 45, 46], of PQ and the FeS center [47], and of PS I [48] in emergence of the slow phase. The slow phase of electrochromic changes

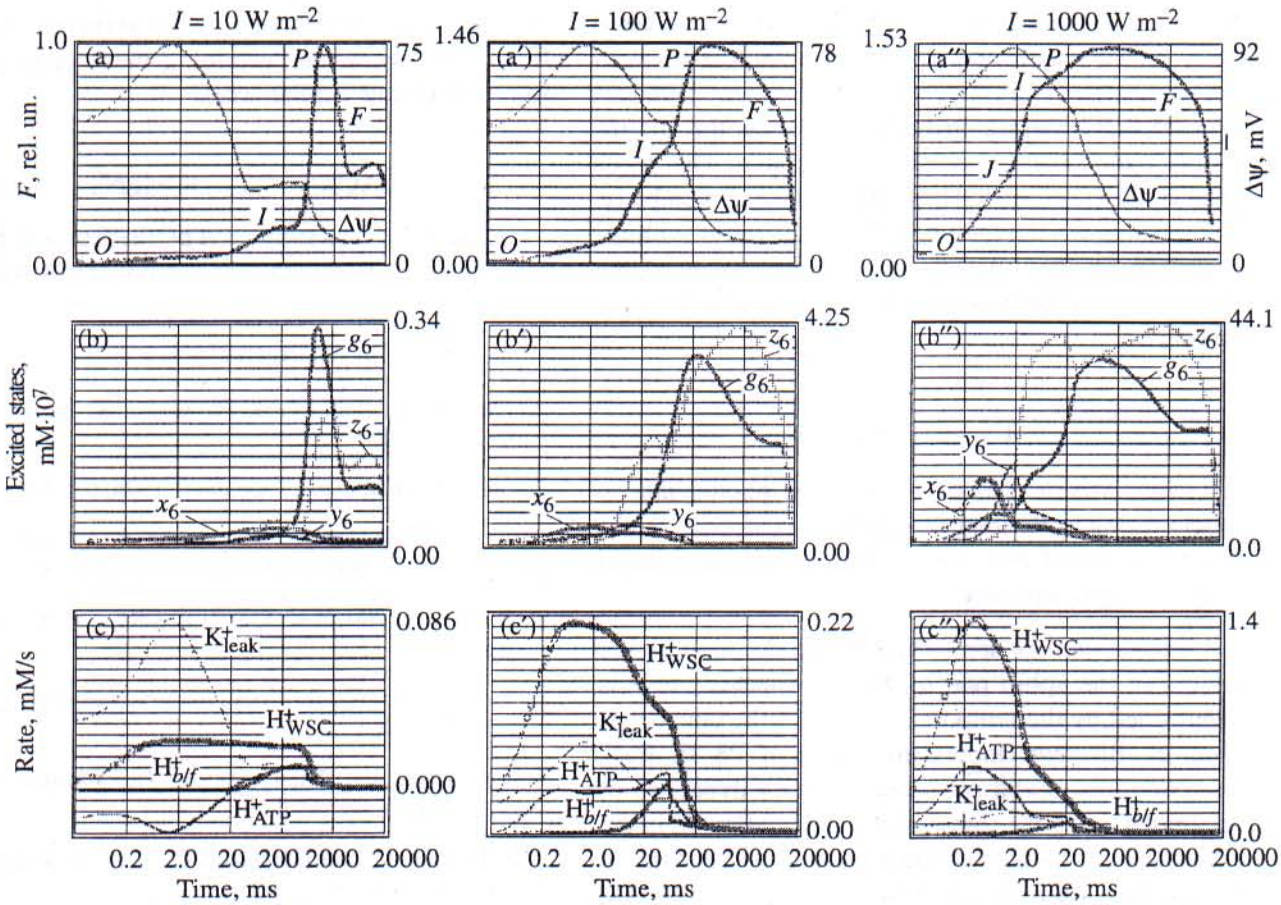

Fig. 6. Induction effects calculated with the proposed model for three illumination level specified at the top of each column. The time scale is logarithmic. Panels (a), relative fluorescence yield (F) and transmembrane electric potential ($\Delta\psi$). Panels (b), concentrations of PS II excited states. Panels (c) rates of processes producing and consuming the electric charge in the thylakoid lumen: $H^+_{b/f}$ is the proton influx from plastoquinol oxidation at the cyt b/f luminal side, H^+_{WSC} is the proton influx from the water-splitting complex; H^+_{ATP} is proton consumption in the ATP synthase reaction; K^+_{lead} is K^+ leakage through the membrane.

was reported to be especially distinct at low light intensity [49].

In terms of our model, $\Delta\psi$ at every moment is determined by the charge difference between lumen and stroma. Figure 6c depicts the time changes in the rates of processes involved in generation and utilization of electric charge in the lumen. Focusing on the left-hand panels of Fig. 6, one can see that emergence of the $\Delta\psi$ 'slow phase' coincides with the establishment of a certain quasi-steady state of the charge-producing system of the thylakoid lumen. The latter means that over the period from ca. 50 to ca. 300 ms the oppositely directed processes largely counterbalance each other. From 50 to 200 ms, the proton influx to the lumen increases owing to plastoquinol oxidation at the luminal side of the b/f complex (Fig. 6c, $H^+_{b/f}$), as the system accumulates states with Q_B^{2-} which upon protonation dissociates from PS II, and accumulation of plastoquinol at the stromal side of the thylakoid membrane 'starts' the b/f complex. The proton influx from the water-splitting complex (H^+_{WSC}) and b/f is balanced by the K^+ leakage (K^+_{lead}) and proton consumption in the ATP synthase reaction (H^+_{ATP}). Besides, a fraction of protons is taken up by the buffer (not shown). As a result, the evolving slow phase in the transmembrane potential kinetics leads to inhibition of electron transfer in potential-dependent reactions of PS II. Such inhibition, in its turn, hinders the rise in the z_6 content to produce the intermediate minimum in its dynamics (Fig. 6b), which ultimately results in appearance of the shoulder (I) on the induction curve (Fig. 6a).

The breakdown of the above-described quasi-steady state over 300–600 ms (Fig. 6c) is in all probability caused by activation of the PS I processes, with enhancement of cyclic electron transfer resulting in

competition for PQ between PS II and the *b/f* complex. As a consequence, PS II accumulates states with vacant Q_B site (*g* family), whereas the extent of reduction of the *b* hemes increases to retard the plastoquinol reoxidation at the *b/f* luminal side. This leads to accumulation of PQH_2 in the thylakoid membrane and ensuing accumulation of the PS II states with reduced Q_B (*z* family). Elevated concentrations of the fluorescing forms g_6 and z_6 results in enhanced fluorescence.

CONCLUSION

Our kinetic model of primary photosynthetic processes has provided a realistic description of the fast induction of chlorophyll fluorescence in a broad range of light intensity.

Modeling has demonstrated that the multiphasic pattern of the uphill part of the fluorescence curve is determined by the temporal changes in the concentrations of different fluorescing forms of PS II. Each level of illumination produces a certain dynamics of accumulation of the fluorescing states, reflected in the characteristic features of the induction curve. Similar results have been obtained by other researchers [13] with a PS II model at high light intensities. Examination of separate blocks of our model demonstrates that to describe the fast phase of induction under intense light it is indeed sufficient to consider only PS II and plastoquinol reoxidation in the PQ pool. However, adequate description of the process under moderate and weak illumination requires consideration of the whole system of generation and utilization of the transmembrane electrochemical proton gradient, including the functioning of the *b/f* complex, PS I, ATP synthase, and passive ion leakage through the thylakoid membrane; furthermore, account should be taken of the inhibition of some electron transfer step by the transmembrane electric potential. Thus we propose a unified model that successfully describes the fast phase of chlorophyll fluorescence induction at any light intensity, as distinguished from the models [11, 13] built for particular cases of only intense or only weak illumination.

Moreover, our model admits analysis of the composition of the fluorescent signal under broadly varied light intensity, as well as detailed investigation of $\Delta\psi$ and ΔpH generation on the thylakoid membrane, ion fluxes, and a number of other important characteristics of primary photosynthetic processes. Testing the model in describing these process is the objective of our further work.

ACKNOWLEDGMENT

The work was supported by the Russian Foundation for Basic Research, project no. 00-04-48919.

REFERENCES

1. Dau, H., *J. Photochem. Photobiol. B: Biology*, 1994, vol. 26, p. 3.
2. Dau, H., *Photochem. Photobiol.*, 1994, vol. 60, pp. 1–23.
3. Krause, G.H. and Weis, E., *Ann. Rev. Plant. Physiol. Plant. Mol. Biol.*, 1991, vol. 42, pp. 313–349.
4. Lazar, D., *Biochim. Biophys. Acta*, 1999, vol. 1412, pp. 1–28.
5. Kautsky, H. and Hirsch, A., *Naturwissenschaften*, 1931, vol. 48, p. 964.
6. Govindjee and Papageorgiou, G., *Photophysiology*, 1971, vol. 6, pp. 1–50.
7. Schreiber, U. and Neubauer, C., *Z. Naturforsch*, 1987, vol. 42, pp. 1255–1264.
8. Neubauer, C. and Schreiber, U., *Z. Naturforsch*, 1987, vol. 42, pp. 1246–1254.
9. Trissl, H.-W., Gao, Y., and Wulf, K., *Biophys. J.*, 1993, vol. 64, pp. 974–988.
10. Renger, G. and Shulze, A., *Photobiochem. Photobiophys*, 1985, vol. 9, pp. 79–87.
11. Baake, E. and Shloeder, J.P., *Bull. Math. Biol.*, 1992, vol. 54, pp. 999–1021.
12. Hsu, B.-D., *Biochim. Biophys. Acta*, 1992, vol. 1140, pp. 30–36.
13. Stirbet, A., Govindjee, Strasser, B.J., and Strasser, R.J., *J. Theor. Biol.*, 1998, vol. 193, pp. 131–151.
14. Kukushkin, A.K. and Tikhonov, A.N., *Biofizika*, 1979, vol. 24, no. 1, pp. 87–91.
15. Kukushkin, A.K. and Tikhonov, A.N., *Lektsii po biofizike fotosinteza vysshikh rastenii* (Lectures on the Biophysics of Higher Plant Photosynthesis), Moscow: Izd. MGU, 1988.
16. Dubinskii, A.Yu. and Tikhonov, A.N., *Biofizika*, 1994, vol. 39, no. 4, p. 652.
17. Karavaev, V.A., *Biofizika*, 1988, vol. 33, no. 5, pp. 876–877.

18. Hsu, B.-D., Lee, Y.-S., and Jang, L.-R., *Biochim. Biophys. Acta*, 1989, vol. 975, pp. 44–49.

19. Vredenberg, W.J., *Biophys. J.*, 2000, vol. 79, pp. 26–38.

20. Lebedeva, G.V., Belyaeva, N.E., Ruznichenko, G.Yu., and Demin, O.V., *BioThermoKinetics in the Post genomic Era*, Larsson, C., Pahlman, I., and Gustafsson, L., Eds., Goteborg: Chalmers Reproservice, 1998, pp. 196–199.

21. Riznichenko, G.Yu., Lebedeva, G.V., Demin, O.V., and Rubin, A.B., *J. Biol. Phys.*, 1999, vol. 25, pp. 177–192.

22. Riznichenko, G.Yu., Lebedeva, G.V., Demin, O.V., Belyaeva, N.E., and Rubin, A.B., *Biofizika*, 2000, vol. 45, no. 3, pp. 452–460.

23. Lebedeva, G.V., Belyaeva, N.E., Riznichenko, G.Yu., Rubin, A.B., and Demin, O.V., *Fiz. Khimiya*, 2000, vol. 74, pp. 1897–1906.

24. Belyaeva, N.E., Demin, O.V., Lebedeva, G.V., Riznichenko, G.Yu., and Rubin, A.B., *Matematika. Komp'yuter. Obrazovanie* (Mathematics, Computer, Education), Moscow: Progress-Traditsiya, 2001, no. 8, pp. 587–595.

25. Rubin, A.B. and Shinkarev, V.P., *Transport elektronov v biologicheskikh sistemakh* (Electron Transport in Biological Systems), Moscow: Nauka, 1984.

26. Malik, M., Riznichenko, G.Yu., and Rubin, A.B., *Biological Electron Transport Processes. Their Mathematical Modeling and Computer Simulation*, Horwood, 1990.

27. Riznichenko, G.Yu., *Matematicheskie modeli pervichnykh protsessov fotosinteza* (Mathematical Models of Primary Photosynthetic Processes), *Itogi Nauki i Tekhniki, Ser. Biofiz.*, Moscow: VINITI, vol. 33, 1991.

28. Hall, D.O. and Rao, K.K., *Photosynthesis. Vth edition. Studies in Biology*, Cambrige University Press, 1994.

29. Hope, A.B., *Biochim. Biophys. Acta*, 1993, vol. 1143, pp. 1–22.

30. Brettel, K., *Biochim. Biophys. Acta*, 1997, vol. 1318, pp. 322–373.

31. Gibasiewicz, K., Dobek, A., Breton, J., and Leibl, W., *Biophys. J.*, 2001, vol. 80, pp. 1617–1630.

32. Reynolds, I.A., Johnson, E.A., and Tanford, C., *Proc. Natl. Acad. Sci. USA*, 1985, vol. 82, p. 6869.

33. Demin, O.V., Westerhoff, H.W., and Kholodenko, B.N., *Biokhimiya*, 1998, vol. 63, p. 755.

34. Skulachev, V.P. and Kozlov, I.A., *Protonnye adenozintrifosfatazy: molekulyarnye biologicheskie generatory toka* (Proton Adenosine Triphosphatases: Molecular Biological Electric Generators), Moscow: Nauka, 1977.

35. Van Kooten, O., Snel, J.F.H., and Vredenberg, W.J., *Photosynth. Res.*, 1986, vol. 9, p. 211.

36. Kholodenko, B.N., Stabilizing regulation in multienzyme systems: modeling of bioenergetic processes, *Doctoral (Phys.–Math.) Dissertation*, Moscow, Belozersky Inst. Phys.-Chem. Biol., MSU, 1988.

37. Boork, J. and Wennestrom, H., *Biochim. Biophys. Acta*, 1984, vol. 767, pp. 314–320.

38. Nicholls, D.G., *Eur. J. Bioch.*, 1974, vol. 50, pp. 305–315.

39. Brown, G.C. and Brand, M.D., *Biochem. J.*, 1986, vol. 234, pp. 75–81.

40. Markin, V.S. and Chizmadzhev, Yu.A., *Indutsirovannyi ionnyi transport* (Induced Ion Transport), Moscow: Nauka, 1974.

41. Schatz, G.H., Brock, H., and Holzwarth, A.R., *Biophys. J.*, 1988, vol. 54, p. 397.

42. Drachev, L.A., Kaurov, B.S., Mamedov, M.D., Mulkidjanian, A.Y., Semenov, A.Y., Shinkarev, V.P., Skulachev, V.P., and Verkhovsky, M.I., *Biochim. Biophys. Acta*, 1989, vol. 973, pp. 189–197.

43. Semenov, A.Y., *FEBS Lett.*, 1993, vol. 321, pp. 1–5.

44. Strasser, R.J., Srivastava, A., and Govindgee, *Photochem. Photobiol.*, 1995, vol. 61, pp. 32–42.

45. Bouge-Bouquet, B., *Biochim. Biophys. Acta*, 1977, vol. 462, pp. 371–379.

46. Crowther, D. and Hind, G., *Arch. Biochem. Biophys.*, 1980, vol. 204, pp. 568–571.

47. Malkin, R., *Proc. 5th. Int. Congr. Photosynth.*, 1981, vol. 2, pp. 643–653.

48. Joliot, P. and Delosme, R., *Biochim. Biophys. Acta*, 1974, vol. 357, pp. 267–284.

49. Bouge-Bouquet, B., *Biochim. Biophys. Acta*, 1981, vol. 635, pp. 327–340.